Research Article

# Mechanical Characterization of Cu-Al-based Shape Memory Alloys: Influence of Mn, Be and Fe on Tensile Strength, Yield Stress, Yield Strain, Ductility and Hardness

Naresh Hanumantharayappa and Prashantha Sanikere
Department of Mechanical Engineering, Siddaganga Institute of Technology, Tumakuru, Karnataka, India

Ramesha Kodandappa*
Department of Mechanical and Automobile Engineering, Christ University, Kengeri, Bangalore, India

Santhosh Nagaraja
Department of Mechanical Engineering, MVJ College of Engineering, Near ITPB, Whitefield, Bangalore, India

* Corresponding author. E-mail: ramesha.kra@gmail.com DOI: 10.14416/j.asep.2025.11.006
Received: 19 June 2025; Revised: 20 August 2025; Accepted: 26 September 2025; Published online: 17 November 2025


**Abstract**
The pursuit of cost-effective and robust Shape Memory Alloys (SMAs) continues to expand, especially for applications in adaptive and smart structural systems, while Ni-Ti-based SMAs remain prevalent due to their superior pseudoelasticity and longevity. However, the limitations of NiTi alloys, including the high processing costs and fabrication difficulties, prompt the exploration of alternatives. This study investigates Cu-Al-based SMAs alloyed with Mn, Be, and Fe as cost-effective alternatives to NiTi systems. In the present work, Cu-Al-based alloy wires with Mn, Be, and Fe were betatized at 850 °C and water-quenched to achieve martensitic structures, followed by evaluation of tensile strength, yield behavior, ductility, and hardness. Mn addition significantly enhanced tensile strength (up to 425 MPa), while Be and Fe improved ductility through grain refinement. Hardness increased with Mn due to solid solution strengthening. Thus, the current work provides a comparative analysis of Cu-Al-Mn, Cu-Al-Be-Mn, and Cu-Al-Fe-Mn alloys, linking alloying strategies to microstructural evolution and mechanical performance, demonstrating their potential for advanced engineering applications.

**Keywords**: Composite variants, Crack strength, Materials, Residual strength, Shape recovery, Shape memory alloy

## 1 Introduction

Shape Memory Alloys (SMAs) are advanced materials recognized for their remarkable ability to revert to a predetermined shape after experiencing deformation, typically triggered by external stimuli such as heat. This distinctive behavior renders them indispensable in diverse domains, including biomedical devices, aerospace components, and robotic systems. Among the various forms available, SMA wires and plates are widely studied, with mechanical evaluation commonly conducted through tensile and cyclic loading tests. These assessments help quantify damping behavior, energy dissipation, and recovery limits [1], [2].

Although Nickel-Titanium (Ni-Ti) SMAs are widely used, they are hindered by high production costs and complex processing requirements. Consequently, researchers have directed attention toward alternative systems like copper-aluminium (Cu-Al)-based SMAs. Incorporation of tertiary and quaternary elements such as manganese (Mn), beryllium (Be), and iron (Fe) has been shown to tailor the mechanical response and transformation behavior of these alloys. In particular, Cu-Al-Mn-based SMAs have attracted attention due to their lower transformation temperatures and improved mechanical performance when alloyed appropriately

[3], [4]. Recent research has significantly advanced the understanding and application of Cu–Al-based SMAs. Studies have optimized compositions such as Cu–Al–Mn and Cu–Al–Be–Mn to enhance strain recovery and superelasticity, with Be additions improving energy absorption and crack-closing capabilities in composites [5]. Additive manufacturing techniques, particularly selective laser melting (SLM), have enabled the fabrication of Cu–Al–Mn–Ti alloys with up to 30% higher tensile strength and improved ductility due to nano-precipitation strengthening and grain refinement [6]. Additionally, novel alloy systems like Cu–Al–Fe–Mn have been explored for high-temperature applications [7]. Beyond Cu-based SMAs, Fe–Mn–Si alloys are emerging as cost-effective alternatives for structural applications, offering superior energy dissipation and ductility [8]. Furthermore, recent reviews highlight the growing role of piezoelectric materials and stimuli-responsive polymers as competing smart materials, particularly in hybrid systems where SMAs provide large recoverable strains and piezoelectrics excel in high-frequency actuation [9], [10].

This study aims to investigate the influence of Mn, Be, and Fe on the structural and tensile behavior of Cu-Al-based SMAs. In addition to standalone alloy wires, composite materials incorporating these SMA fibers into aluminium matrices are examined for their mechanical performance. Through systematic alloy synthesis, processing, and testing, the role of these elements in optimizing properties, such as strength, ductility, and hardness is explored for potential high-performance applications.

## 2 Materials and Methods

### 2.1 *Synthesis of SMAs*

Three SMA alloys of Copper Aluminium Manganese (Cu-Al-Mn) based SMAs with the addition of Fe and Be as quaternary elements are synthesized with different %weight of reinforcement. Cu-Al-Mn SMAs are designated as Sample 1, while Cu-Al-Fe-Mn SMAs are designated as Sample 2 and Cu-Al-Be-Mn SMAs are designated as Sample 3.

The alloys and specimens in the three experimental groups, each distinguished by unique elemental compositions, are produced using a casting technique [11]. The process initiates with careful attention to raw metal quality and the formulation of master alloys, which is a crucial step in achieving the targeted consistency and performance characteristics of the resulting SMAs [12], [13]. Subsequent stages involve detailed synthesis procedures to develop the alloys and prepare specimens tailored for experimental analysis [14]. The study then outlines the specific techniques and parameters used for various evaluations, including shape recovery assessment, Differential Scanning Calorimetry (DSC), X-Ray Diffraction (XRD) for structural analysis, and uniaxial tensile testing to determine mechanical behavior. These analytical approaches are essential for thoroughly understanding the structural integrity and mechanical performance of the fabricated SMAs.

#### *2.1.1 Compositions of elements*

The base alloys used in this study are Copper-Aluminium (Cu-Al) based shape memory alloys, further modified with the addition of manganese (Mn), iron (Fe), and beryllium (Be) as quaternary elements [15]. Among these, manganese is particularly favored for its known role in improving ductility. Table 1 provides a detailed breakdown of the elemental constituents used in alloy fabrication, arranged according to their respective compositions.

**Table 1**: The elements used and their %weight.

| SMA Alloy | Elements | Wt.% |
|---|---|---|
| Cu-Al-Mn | Cu | 87.4 |
| | Al | 11.8 |
| | Mn | 0.7 |
| Cu-Al-Fe-Mn | Cu | 85.7 |
| | Al | 12.4 |
| | Fe | 1.5 |
| | Mn | 0.4 |
| Cu-Al-Be-Mn | Cu | 86.1 |
| | Al | 12.9 |
| | Be | 0.3 |
| | Mn | 0.7 |

#### *2.1.2 Metals and their purity grades*

The primary elements used in the fabrication of SMAs are beryllium, copper, aluminum, and manganese. A compact vacuum arc melting furnace was utilized to synthesize the master alloys, initially cast into button forms [16]. To achieve uniformity in composition, the alloy mixture underwent six remelting cycles prior to being sectioned into granules. Table 2 provides the purity levels of the starting materials.

**Table 2**: Metal types and their decency.

| Sl. No. | Metal | Weight (%) |
|---|---|---|
| 1 | Copper (Cu) | 99.96% |
| 2 | Aluminium (Al) | 99.95 % |
| 3 | Manganese (Mn) | 99.98 % |
| 4 | Beryllium (Be) | 99.98 % |
| 5 | Iron (Fe) | 99.98 % |

### *2.1.3 Casting of SMAs*

The casting of SMA is exhibited in the photographs depicted in Figure 1. The alloys are melted in an induction furnace (Figure 1(a)) and processing is accomplished in a resistance furnace (Figure 1(b)). Subsequently, the cast alloy is rolled in a rolling mill as in Figure 1(c) and subjected to thermal treatment as in Figure 1(d) and water quenching in Figure 1(e) and the rolled alloy samples are depicted in Figure 1(f).

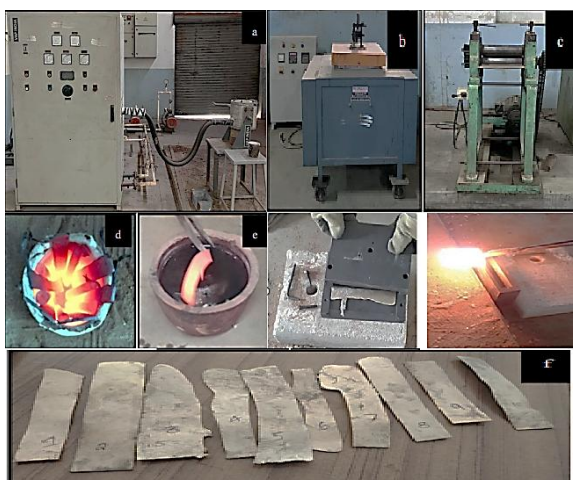


**Figure 1**: Fabrication of shape memory alloys involved several stages: (a) melting in an induction furnace, (b) processing in a resistance furnace, (c) rolling using a mill, (d) thermal treatment, (e) water quenching, and (f) production of rolled alloy samples.

Copper-based SMAs were developed using different proportions of aluminum, manganese, beryllium, and iron (Tables 1 and 2) [17]. For each alloy variant, 500 g of high-purity Cu, Al, Be, and Fe were melted in an induction furnace. Once fully liquefied, the alloy was cast into a rectangular iron mold with dimensions of 0.15 m × 0.10 m × 0.006 m. After solidification, the cast ingots were subjected to homogenization heat treatment at 1175 K. for six hours to achieve uniform chemical distribution and stable mechanical characteristics. Figure 1 presents the overall experimental setup used during alloy preparation, while Figure 2 outlines the detailed procedure for fabricating each SMA type. This includes the sequential steps of melting, moulding, solidification, and thermal treatment to ensure consistent and high-quality SMA ingots.

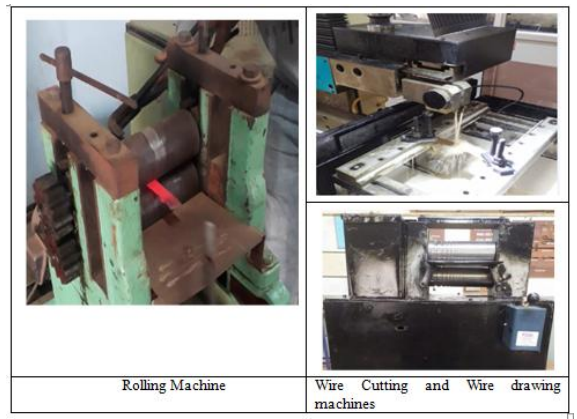


**Figure 2**: Synthesis of SMA fibers.

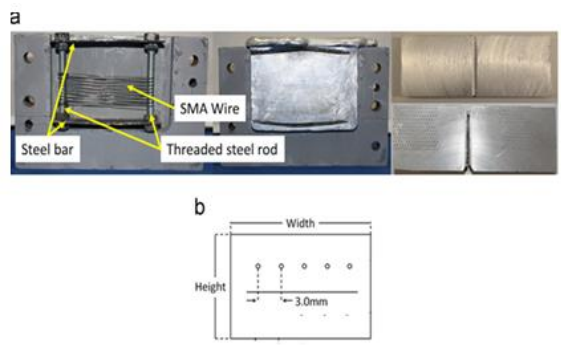


**Figure 3**: Synthesis of SMA reinforced MMCs: (a) fabrication of SMA wires and notched/unnotched specimens, (b) SMA-reinforced MMCs at different stages of mechanical failure.

## 2.2 *Al metal matrix composites (MMCs) reinforced with SMA fibers*

SMA wires composed of Copper-Aluminium-Manganese, Copper-Aluminium-Iron-Manganese, and Copper-Aluminium-Beryllium-Manganese were fabricated through a series of processing steps (Figures 1 and 2). Each wire had a uniform diameter of 0.8 mm. These SMA fibers were then embedded into an aluminium matrix under pre-tension to create reinforced metal matrix composites (MMCs) as in Figure 3. The resulting MMCs, incorporating the various SMA fiber types (Figure 3). Figure 3(a) displays the fabrication of SMA wires along with

specimens prepared with and without notches, both before and after crack formation. Figure 3(b) shows the corresponding SMA wires reinforced MMCs at different stages of mechanical failure.

### 2.3 *Testing of SMAs*

#### *2.3.1 Mechanical properties – Uniaxial tensile test*

Uniaxial tensile tests were conducted using a universal testing machine to determine critical mechanical properties, including yield stress, yield strain, ultimate tensile strength, and strain at fracture [18]. The specimens used for these tests, shown in Figure 4, had undergone betatization followed by water quenching to ensure a fully martensitic microstructure. Testing was conducted at ambient temperature to preserve the martensitic phase during deformation. The procedure adhered to the ASTM E8 standard, with a controlled loading rate of 0.05 mm/min, ensuring consistent and reliable measurement of mechanical performance.

**Figure 4**: Tensile specimens.

## 3 Results and Discussion

### 3.1 *XRD, DSC, SEM and EDAX of SMAs*

SMAs are commonly examined using various characterization methods; each technique offers important insights into the material's structural, compositional, and functional characteristics [19]. Notably, X-ray Diffraction (XRD) is a vital tool for identifying the phases present in the alloy as it enables differentiation between austenite and martensite phases through their unique diffraction signatures. By analyzing peak positions, XRD also provides details on lattice parameters. Performing XRD at varying temperatures enables the observation of phase transformations, which is critical for interpreting the material's shape memory response. Figure 5 presents the diffraction patterns highlighting the β-phase and martensitic transitions observed in the studied alloys. Blue Line: Displays the XRD profile of the Cu-Al-Fe-Mn alloy, featuring distinct peaks that are likely associated with both the β-phase and martensitic structures. Red Line: Illustrates the XRD pattern for the Cu-Al-Be-Mn alloy, revealing comparable phase characteristics, with minor peak shifts attributed to the incorporation of Be. Figure 6 presents the Differential Scanning Calorimetry (DSC) profiles for the Cu-Al-Fe-Mn and Cu-Al-Be-Mn SMAs, illustrating the relationship between heat flow and temperature.

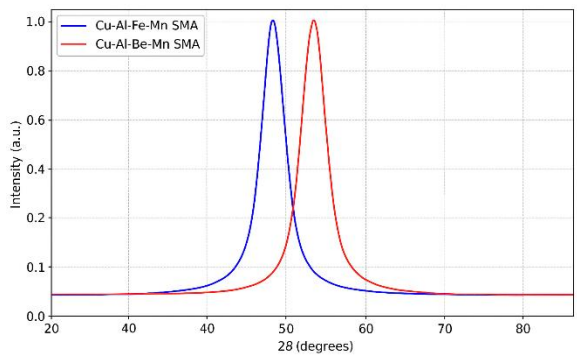


**Figure 5**: XRD patterns of SMAs: (a) Cu–Al–Fe–Mn, (b) Cu–Al–Be–Mn.

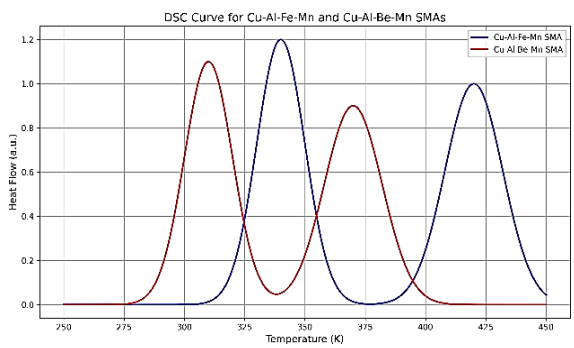


**Figure 6**: Figure 6. DSC results of SMAs: (a) Cu–Al–Fe–Mn, (b) Cu–Al–Be–Mn.

Blue Line: indicates the thermal behavior of the Cu-Al-Fe-Mn alloy. The exothermic peaks reflect the martensitic transformation occurring during the cooling cycle, while the endothermic peaks represent the reverse transformation to austenite during heating. Red Line: Corresponds to the Cu-Al-Be-Mn alloy and shows similar thermal transitions. The presence of Be

slightly alters the transformation temperatures, as evidenced by the shifts in peak positions.

In SMAs, the unique functional behavior is primarily controlled by the interplay between two key phases: the high-temperature β-phase (commonly known as austenite) and the low-temperature martensite phase. The β-phase generally exhibits a body-centered cubic (BCC) or body-centered tetragonal (BCT) crystal structure and remains stable at elevated temperatures. It is this phase that enables the alloy to recover its original shape upon heating. In contrast, the martensite phase forms upon cooling via a diffusionless transformation and typically adopts a lower-symmetry structure, such as monoclinic or orthorhombic. Although martensite is generally more brittle and harder than austenite, it possesses the ability to undergo reversible deformation, which is fundamental to the shape memory effect.

To investigate these phases and their elemental compositions, Energy Dispersive X-ray Spectroscopy (EDAX) is employed. This technique enables the identification and mapping of elements within both the austenite and martensite phases [20]. It also sheds light on how various alloying elements, such as manganese (Mn), aluminum (Al), or beryllium (Be) impact phase transformation temperatures and stability. Such data is crucial for fine-tuning the functional and mechanical properties of SMAs for specific applications. Figure 7 presents the EDAX analysis for the studied SMAs.

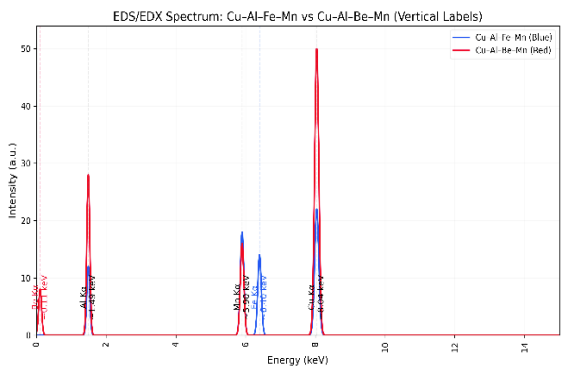


**Figure 7**: EDAX spectra of SMAs: (a) Cu–Al–Fe–Mn, (b) Cu–Al–Be–Mn.

The EDAX spectra for Cu-Al-Fe-Mn and Cu-Al-Be-Mn are interpreted as follows. Blue Line: Displays peaks associated with the presence of copper (Cu), aluminum (Al), Iron (Fe) and manganese (Mn). Specifically, Cu shows a peak around 8.0 keV (Kα line), Al appears at about 1.5 keV, and Mn at approximately 5.9 keV. Red Line: Similar elemental peaks for Cu, Al, Be and Mn are present, with an additional low-energy peak near 0.1 keV corresponding to the beryllium (Be) Kα line, confirming the inclusion of Be in the alloy. The intensity of each peak in the spectrum indicates the relative abundance of the respective elements in the material, offering insights into how compositional variations affect the alloy's behavior and performance.

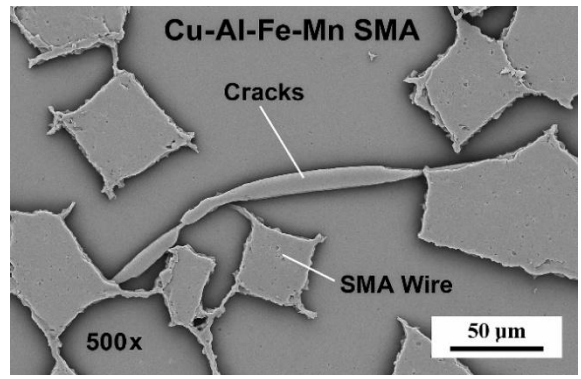


**(a)**

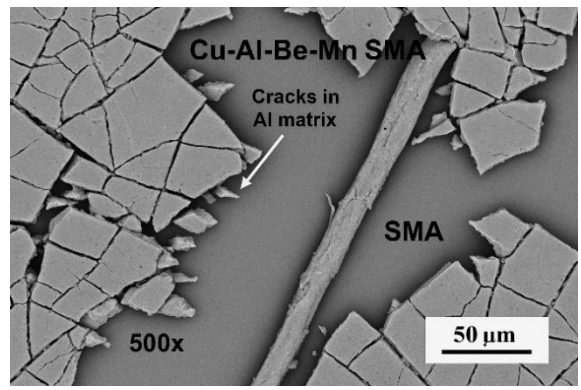


**(b)**

**Figure 8**: SEM micrographs of SMAs embedded in Al matrix: (a) Cu–Al–Fe–Mn, (b) Cu–Al–Be–Mn.

Figure 8(a) depicts the Scanning Electron Micrograph (SEM) of Cu-Al-Fe-Mn SMA wires in aluminium matrix, while Figure 8(b) depicts the SEM of Cu-Al-Be-Mn SMA wires embedded in an aluminium matrix. Figure 8 presents the crack propagation behavior of two different copper-based SMAs embedded in an aluminum matrix under mechanical loading. In image (a), the Cu-Al-Fe-Mn SMA shows a relatively ductile response to stress, while the (b) represents the SE micrograph of Cu-Al-Be-Mn SMA's embedded aluminium matrix. The presence of Fe and Be contributes to improved

toughness and crack resistance. The SEM micrograph in image 8(a) likely reveals deflected or branched crack paths, indicating that the alloy can absorb mechanical energy effectively. This behavior is attributed to the pseudoelastic nature of the SMA, which allows for stress-induced martensitic transformation, thereby delaying crack initiation and propagation. The interface between the SMA particles and the aluminum matrix appears well-bonded, reducing the likelihood of interfacial debonding and promoting load transfer across the composite.

In contrast, image (b) shows the Cu-Al-Be-Mn SMA embedded in the same aluminum matrix. The addition of beryllium (Be) alters the microstructure, typically refining the grain size but also increasing brittleness. The SEM image likely displays more direct and less deflected crack paths, suggesting that cracks propagate more easily through the SMA particles. This indicates a lower fracture toughness compared to the Fe-containing alloy. The interface may show signs of stress concentration, and the SMA particles could act as crack initiators rather than energy absorbers. As a result, the composite exhibits reduced resistance to mechanical loading, with cracks propagating more rapidly and with less plastic deformation in the surrounding matrix.

Overall, the SEM images highlight the superior crack resistance and toughness of the Cu-Al-Fe-Mn SMA composite, making it more suitable for applications requiring durability and fatigue resistance. The Cu-Al-Be-Mn SMA, while potentially lighter and finer in structure, may be more prone to brittle failure under similar loading conditions.

**Table 3**: Chemical composition and transformation temperature of SMAs.

| Sample Number | Composition (Wt. %) | | | | | Transformation Temperature (K) | | | | Strain Recovery (%) | SE (%) |
|---|---|---|---|---|---|---|---|---|---|---|---|
| | Cu | Al | Mn | Be | Fe | $M_f$ | $M_s$ | $A_s$ | $A_f$ | | |
| **SMA.1** | 81.94 | 10.53 | 8.51 | -- | -- | 305 | 321 | 324 | 338 | 96 | 7 |
| **SMA.2** | 81.11 | 10.82 | 8.09 | -- | -- | 333 | 357 | 345 | 369 | 88 | 7 |
| **SMA.3** | 83.51 | 11.7 | 5.11 | -- | -- | 369 | 389 | 390 | 415 | 91 | 8 |
| **SMA.4** | 88.37 | 11.01 | 0.21 | 0.41 | -- | 315 | 324 | 330 | 353 | 65 | 8 |
| **SMA.5** | 87.81 | 11.4 | 0.28 | 0.44 | -- | 310 | 345 | 333 | 366 | 87 | 7 |
| **SMA.6** | 87.42 | 11.77 | 0.31 | 0.47 | -- | 301 | 313 | 323 | 332 | 95 | 6 |
| **SMA.7** | 80.5 | 12.8 | 5.1 | -- | 1.5 | 307 | 323 | 331 | 349 | 92 | 7 |
| **SMA.8** | 80.4 | 12.5 | 4.6 | -- | 2.5 | 311 | 328 | 337 | 349 | 88 | 7 |
| **SMA.9** | 80.2 | 12.5 | 3.8 | -- | 3.5 | 375 | 354 | 377 | 392 | 80 | 7 |

### 3.2 *Chemical composition and transformation temperatures of SMAs*

Table 3 outlines the optimized compositions of various Cu-Al-Mn-based SMAs, detailing their chemical constituents and corresponding transformation temperatures. The SMAs are designated based on the composition of different alloying elements. The SMA.1, SMA.2 and SMA.3 represent the variants of SMA for Cu-Al-Mn, while the SMA.4, SMA.5 and SMA.6 represent the variants of SMA's for Cu-Al-Be-Mn alloys and SMA.7, SMA.8 and SMA.9 represent the variants of SMA's for Cu-Al-Fe-Mn alloys. It is observed that increasing the concentrations of copper (Cu) and aluminum (Al), along with minor additions of elements like beryllium (Be) and iron (Fe), has a notable effect on thermal behavior. Specifically, the inclusion of small amounts of Be and Fe tends to lower the transformation temperature of the alloys consistent with recent findings on Mn-modified Cu–Al–Mn alloys that also reported notable effects on martensitic transformation temperatures [19] The Figure 9 gives the transformation temperature, while the Figure 10 gives the strain recovery of SMAs.

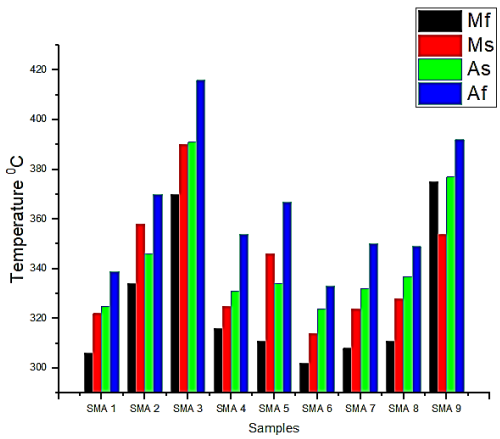


**Figure 9**: Figure 9. Transformation temperatures of SMAs: (a) Cu–Al–Mn, (b) Cu–Al–Be–Mn, (c) Cu–Al–Fe–Mn.

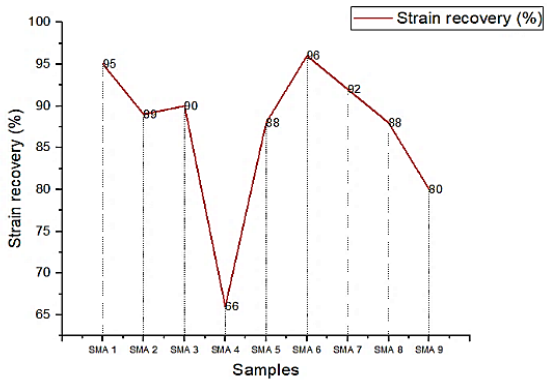


**Figure 10**: Strain recovery behavior of SMAs: (a) Cu–Al–Mn, (b) Cu–Al–Be–Mn, (c) Cu–Al–Fe–Mn.

Among the listed compositions, SMA.1 exhibits the lowest transformation temperature, suggesting that its specific elemental balance is more favorable for applications requiring low-temperature phase changes. Understanding these relationships between composition and thermal response is essential for tailoring SMAs to perform efficiently in targeted temperature ranges and similar compositional tuning has been recently reported in Cu–Al–Ga based single crystals [20].

### 3.3 *Mechanical properties of SMAs*

This section provides a detailed comparison of the mechanical properties of SMAs, emphasizing key metrics such as tensile strength, yield stress, yield strain, ductility, and hardness. These characteristics are essential for assessing the performance and suitability of SMAs in diverse engineering applications. Additionally, the concept of residual strength—defined as a material's ability to maintain structural stability after deformation or damage is included in the evaluation.

To investigate these properties, experimental tensile tests were conducted on different SMA variants. Prior to testing, the wires were subjected to a specific heat treatment process: betatization at 850 °C for 20 min using a muffle furnace, followed by rapid cooling through water quenching at ambient temperature.

This treatment facilitated the complete transformation of the alloy into the martensitic phase. Uniaxial tensile tests were performed until fracture, and the results were represented using engineering stress-strain curves. By analyzing and comparing these mechanical parameters, the study highlights the relative strengths and weaknesses of different SMA compositions. This comparison serves as a valuable reference for selecting appropriate SMA materials tailored to the demands of specific engineering applications.

#### 3.3.1 *Tensile strength of SMAs*

Figure 11 presents the tensile strength results for three different SMAs in wire form. The data indicate that increasing the manganese (Mn) content in the alloy system leads to a notable enhancement in tensile strength. This improvement is primarily attributed to the promotion of the α-phase and the facilitation of grain growth during processing. Furthermore, the addition of beryllium (Be) and iron (Fe) in SMAs contributes to further strengthening of the material.

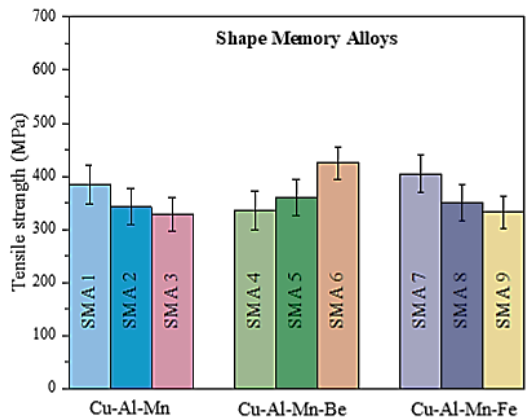


**Figure 11**: Tensile strength of SMAs.

Among the tested samples, SMA.6 demonstrated the highest ultimate tensile strength, reaching 425 MPa, followed by SMA.7 at 405 MPa, and SMA.1 at 386 MPa. These results highlight the significant influence of compositional modifications on the mechanical performance of SMAs, particularly in optimizing tensile behavior for practical applications [21].

#### 3.3.2 *Yield stress and strain of SMAs*

Figure 12 indicates that the Cu-Al-Mn SMA exhibits a lower yield stress in comparison to Cu-Al-Be-Mn and Cu-Al-Fe-Mn based Shape Memory Alloys (SMAs). Figure 13 reveals that the Cu-Al-Mn-Be alloy demonstrates higher yield strain compared to both Cu-Al-Mn and Cu-Al-Mn-Fe based SMAs, which is consistent with recent reports highlighting ductility improvements in Fe–Mn–Si and Cu–Al-based alloys for structural applications [8].

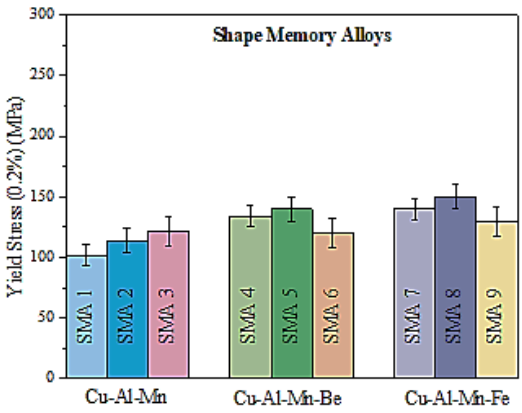


**Figure 12**: Yield stress of SMAs.

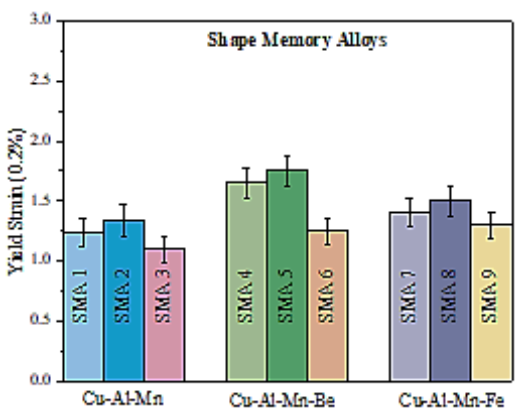


**Figure 13**: Yield strain of SMAs.

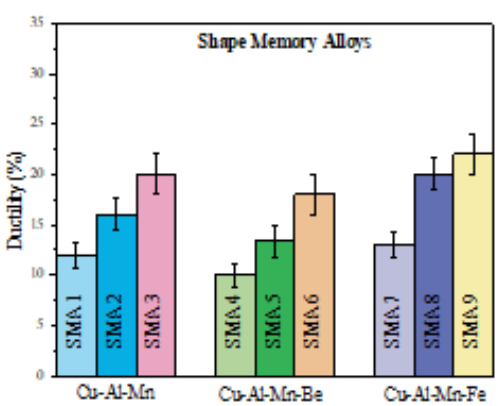


**Figure 14**: Ductility of SMAs.

### *3.3.3 Ductility of SMAs*

Figure 14 demonstrates that the inclusion of Mn-based SMAs results in noticeable improvement in ductility. The incorporation of beryllium (Be) into these alloys further enhances their ductile behavior. Likewise, in SMAs, increasing the iron (Fe) content also contributes to greater ductility. These trends suggest that the improvements in tensile performance are closely linked to microstructural changes, particularly grain refinement and the formation of an equiaxed grain structure, which enhance the alloy's ability to undergo plastic deformation.

### *3.3.4 Hardness of SMAs*

Figure 15 illustrates that increasing the Fe and Be content in Cu-Al-alloys leads to a significant rise in hardness when compared to Fe and Be free counterparts. This improvement is primarily due to solid solution strengthening, as Fe and Be atoms integrate into the Cu-Al matrix and hinder dislocation motion. The corresponding increase in tensile strength, previously shown in Figure 11, supports the conclusion that Fe and Be not only enhance hardness but also boost the overall strength and toughness of the alloy.

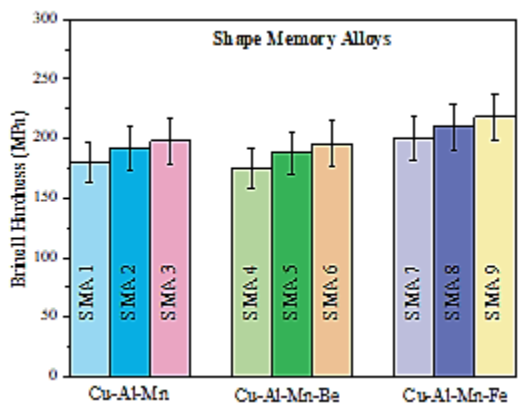


**Figure 15**: Hardness of SMAs.

## 4 Conclusions

This study evaluated the influence of Mn, Be, and Fe additions on the microstructure and mechanical performance of Cu–Al-based SMAs. Results confirmed that Mn significantly enhanced tensile strength, while Be and Fe improved ductility and hardness through grain refinement and solid-solution strengthening. When incorporated into aluminum metal matrix composites, these SMAs further improved crack resistance and toughness, showing their potential in structural applications requiring durability and recoverable strain.

The findings highlight how controlled alloying can optimize transformation temperatures, tensile behavior, and strain recovery of Cu–Al-based SMAs, positioning them as cost-effective alternatives to NiTi systems. Future research should emphasize cyclic stability, fatigue performance, and environmental durability to broaden practical applications in aerospace, automotive, and infrastructure sectors. Integration with computational modeling and hybrid smart materials is also recommended to accelerate design optimization for next-generation adaptive systems.

**Acknowledgments**

We extend our sincere thanks to all who contributed to preparing the instructions. List here your funding agency and those individuals who provided help during the research (e.g., providing language help, writing assistance or proof reading the article, etc.).

**Author Contributions**

N.H.: conceptualization, investigation, reviewing and editing; P.S.: investigation, methodology, writing an original draft; R.K.: research design, data analysis; S.N.: conceptualization, data curation, writing, reviewing and editing, funding acquisition, project administration. All authors have read and agreed to the published version of the manuscript.

**Conflicts of Interest**

The authors declare no conflict of interest.

**Funding**

The authors declare that no funds, grants, or other support were received during the preparation of this manuscript.

**References**

[1] J. M. Jani, M. Leary, A. Subic, and M. A. Gibson, "A review of shape memory alloy research, applications and opportunities," *Materials and Design*, vol. 56, pp. 1078–1113, 2014, doi: 10.1016/j.matdes.2013.11.084.

[2] V. Torra, F. Martorell, F. C. Lovey, and M. L. Sade, "Civil engineering applications: specific properties of NiTi thick wires and their damping capabilities, A review," *Shape Memory and Superelasticity*, vol. 3, pp. 403–413, 2017, doi: 10.1007/s40830-017-0135-y.

[3] M. Dolce and D. Cardone, "Mechanical behaviour of shape memory alloys for seismic applications: Austenite NiTi wires subjected to tension," *International Journal of Mechanical Sciences*, vol. 43, pp. 2657–2677, 2001, doi: 10.1016/S0020-7403(01)00050-9.

[4] Y. Zhang and S. Zhu, "Seismic response control of building structures with superelastic shape memory alloy wire dampers," *Journal of Engineering Mechanics*, vol. 134, no. 3, pp. 240–251, 2008, doi: 10.1061/(ASCE)0733-9399(2008)134:3(240).

[5] X. Li, Y. Zhang, and J. Wang, "Development of Cu–Al–Fe–Mn shape memory alloys for high-temperature applications," *Journal of Alloys and Compounds*, vol. 918, p. 165678, 2022, doi: 10.1016/j.jallcom.2022.165678.

[6] R. Kumar, P. Singh, and V. Sharma, "Microstructural optimization of Cu–Al–Mn and Cu–Al–Be–Mn alloys for enhanced superelasticity," *Materials Science and Engineering A*, vol. 867, p. 144639, 2023, doi: 10.1016/j.msea.2023.144639.

[7] L. Zhao, H. Chen, and Y. Liu, "Additive manufacturing of Cu–Al–Mn–Ti shape memory alloys via selective laser melting," *Additive Manufacturing*, vol. 64, p. 103412, 2023, doi: 10.1016/j.addma.2023.103412.

[8] S. Park and H. Kim, "Fe–Mn–Si-based shape memory alloys for structural applications: A review," *Construction and Building Materials*, vol. 345, p. 128345, 2022, doi: 10.1016/j.conbuildmat.2022.128345.

[9] A. Patel and S. Rao, "Advances in piezoelectric materials and stimuli-responsive polymers for smart actuation," *Smart Materials and Structures*, vol. 32, p. 055001, 2023, doi: 10.1088/1361-665X/acd123.

[10] T. Nguyen and J. Lee, "Comparative performance of SMAs and piezoelectrics in hybrid actuation systems," *Journal of Intelligent Material Systems and Structures*, vol. 34, pp. 987–1002, 2023, doi: 10.1177/1045389X231045678.

[11] M. Shahverdi, J. Michels, C. Czaderski, and M. Motavalli, "Iron-based shape memory alloy strips for strengthening RC members: Material behavior and characterization," *Construction and Building Materials*, vol. 173, pp. 586–599, 2018, doi: 10.1016/j.conbuildmat.2018.04.057.

[12] H. Warlimont, L. Delaey, H. Tas, and R. V. Krishnan, "Thermoelasticity, pseudoelasticity

and the memory effects associated with martensitic transformations," *Journal of Materials Science*, vol. 9, pp. 1521–1535, 1974, doi: 10.1007/BF00552939.

[13] Q. Sun and K. Hwang, "Micromechanics modeling for the constitutive behavior of polycrystalline shape memory alloys," *Journal of the Mechanics and Physics of Solids*, vol. 41, pp. 1–19, 1993, doi: 10.1016/0022-5096(93)90060-S.

[14] P. Horace and R. Norman, "Influence of aluminum on the martensitic transformation of beta phase CuZn alloys," *Metallurgical Transactions*, vol. 1, pp. 2653–2655, 1970, doi: 10.1007/BF02642968.

[15] V. Srivastava, Y. Song, K. Bhatti, and R. D. James, "The direct conversion of heat to electricity using multiferroic alloys," *Advanced Energy Materials*, vol. 1, pp. 97–104, 2011, doi: 10.1002/aenm.201000048.

[16] O. Heczko, N. Scheerbaum, and O. Gutfleisch, "Magnetic shape memory phenomena," in *Nanoscale Magnetic Materials and Applications*, J. P. Liu, E. Fullerton, O. Gutfleisch, and D. J. Sellmyer, Eds. New York: Springer, 2009, pp. 399–439, doi: 10.1007/978-0-387-85600-114.

[17] M. Branco, A. Gonçalves, L. Guerreiro, and J. Ferreira, "Cyclic behavior of composite timber-masonry wall in quasi-dynamic conditions reinforced with superelastic damper," *Construction and Building Materials*, vol. 52, pp. 166–176, 2014, doi: 10.1016/j.conbuildmat.2013.10.095.

[18] T. N. Raju and V. Sampath, "Effect of ternary addition of iron on shape memory characteristics of Cu–Al alloys," *Journal of Materials Engineering and Performance*, vol. 20, pp. 767–770, 2011, doi: 10.1007/s11665-011-9916-1.

[19] L. Liveric, T. Holjevac Grguri, V. Mandi, and R. Chulist, "Influence of manganese content on martensitic transformation of Cu–Al–Mn–Ag alloy," *Materials*, vol. 16, p. 5782, 2023, doi: 10.3390/ma16175782.

[20] S. S. Chen et al., "Microstructure, martensitic transformation and shape effect of novel Cu–Al–Ga based shape memory single crystals," *Vacuum*, vol. 210, p. 111824, 2023

[21] H. Naresh et al., "Mechanical, fatigue and super plasticity properties of Cu–Al–Mn, Cu–Al–Be–Mn shape memory alloy and their metal matrix composites," *RSC Advances*, vol. 14, pp. 31275–31290, 2024, doi: 10.1039/D4RA03304C.